Ligia R. Gomes, John N. Low*, Tanja van Mourik, Herbert Früchtl, Marcus V.N. de Souza, Cristiane F. da Costa and James L. Wardell*

Different substituent effects on the supramolecular arrays in some (*E*)-halo- and nitro-benzaldehyde oximes: confirmation of attractive π(C=N) ··· π(phenyl) interactions

https://doi.org/10.1515/znb-2018-0222
Received October 5, 2018; accepted February 20, 2019

Abstract: The crystal structures and Hirshfeld surface analyses are reported for four aldoximes, (*E*)-X–C_6H_4CH=N–OH [X = 3-Cl (**1**), 4-F (**2**), 2-O_2N (**3**) and 4-O_2N (**4**)]. The strong classical O–H ··· N hydrogen bonds involving the oxime group generate C(3) chains in compound **1**, in contrast to the $R^2_2(6)$ dimers formed in compounds **2–4**; such arrangements have been shown to be the most frequently found for oximes other than salicylaldoximes (2-hydroxybenzaldehyde oximes). In general, weaker intermolecular interactions involving the X substituents, as well as C–H ··· O and π ··· π interactions have significant effects on the supramolecular arrays generated in the aggegation. A further important interaction in compound **1**, and to a lesser extent in compound **4**, is a π(C=N) ··· π(phenyl) molecular stacking. A data base search has indicated that short Cg(C=N) ··· Cg(phenyl) distances, <3.3 Å (Cg = centre of gravity), have been found in various compounds, including other oximes. A theoretical study was carried out starting from the crystal structure data of compound **1**, with optimisation at the BLYP-D3/def2-DZVP level, as well as at the higher PBE0/ma-def2-TZVP level. Breakdown of the interaction energy into separate contributions was achieved using SAPT (using the jun-cc-pvdz basis set). Overall, the calculations indicate that the π(C=N) ··· π(phenyl) interaction is attractive, with a magnitude of 14–18 kJ mol^{-1}.

Keywords: π(C=N) ··· π(phenyl) interactions; aldoximes; crystal structures; quantum chemical calculations.

***Corresponding authors: John N. Low,** Department of Chemistry, University of Aberdeen, Meston Walk, Old Aberdeen, AB24 3UE, Scotland, UK, e-mail: jnl111@gmail.com; and **James L. Wardell,** Department of Chemistry, University of Aberdeen, Meston Walk, Old Aberdeen, AB24 3UE, Scotland, UK; and Instituto de Tecnologia em Fármacos e Farmanguinhos, Fundação Oswaldo Cruz, 21041-250 Rio de Janeiro, RJ, Brazil, e-mail: j.wardell@abdn.ac.uk
Ligia R. Gomes: FP-ENAS-Faculdade de Ciências de Saúde, Escola Superior de Saúde da UFP, Universidade Fernando Pessoa, Rua Carlos da Maia, 296, P-4200-150 Porto, Portugal; and REQUIMTE, Departamento de Química e Bioquímica, Faculdade de Ciências da, Universidade do Porto, Rua do Campo Alegre, 687, P-4169-007 Porto, Portugal
Tanja van Mourik and Herbert Früchtl: School of Chemistry, University of St. Andrews, North Haugh, St. Andrews, Fife KY16 9ST, Scotland, UK
Marcus V.N. de Souza and Cristiane F. da Costa: Instituto de Tecnologia em Fármacos e Farmanguinhos, Fundação Oswaldo Cruz, 21041-250 Rio de Janeiro, RJ, Brazil

1 Introduction

The oxime group, R^1R^2C=NOH, is found in many biologically active compounds [1, 2], with a wide range of uses including as antitumor agents [3–6], acaricides and insecticides [7], thymidine phosphorylase inhibitors [8], anti-microbial agents [9], bactericides [10] and anti-inflammatory agents [11], as well as in the treatment of nerve-gas poisoning [12–15]. In the plant kingdom, oximes play vital metabolic roles [16]. As an important group of organic compounds, it is not surprising that crystal structures of aldoximes have attracted attention [16–19], with well over 60 structures listed in the CCDC data base.

Benzaldehyde oximes, ArCH=NOH, with their -CH=N–OH functional group are ideally arranged for classical O–H ··· O and/ or O–H ··· N hydrogen bonding. The last survey of the classical hydrogen bonding patterns in benzaldehyde oximes reported in 2010 [19] confirmed the most frequently found arrangements, with the exception of salicylaldoxines, were $R^2_2(6)$ dimers and C(3) chains, Fig. 1. Aakerby et al. in 2013 reported the percentages of $R^2_2(6)$ dimers and C(3) chains found in non-salicylaldoxine to be ca.72 and 24%, respectively [20], and similar percentages can be concluded from the most recent survey carried out on June 1st, 2018. The remaining percentage is taken up mainly by compounds in which the oxime group preferentially interacts with an acceptor substituent in the aryl unit, for example as found in pyridinyl compounds [20]. However for other heteroaromatic aldoximes (furanyl, thienyl and pyrrolyl derivatives), as we recently reported, C(3) chains are formed [21].

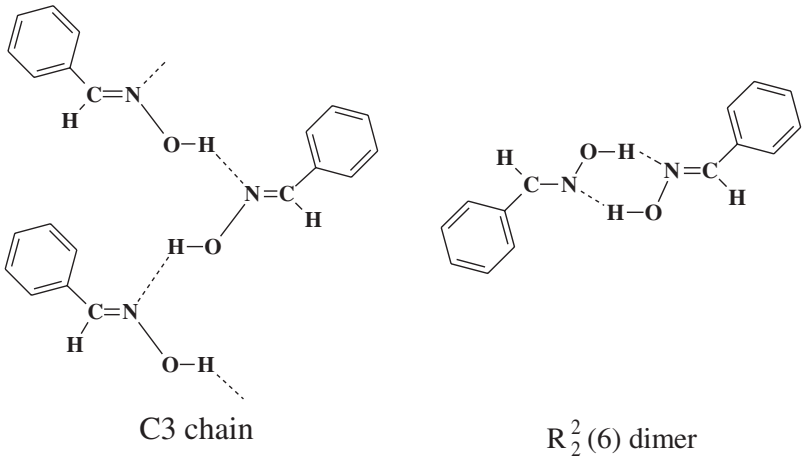

Fig. 1: Illustrations of the C3 chains and $R_2^2(6)$ dimers formed by oximes.

Hydrogen bonds are considered as the strongest and most directional of intermolecular interactions available in molecules [22] and thus play the major role in determining the overall supramolecular structures. However, the involvement of weaker intermolecular interactions, such as C–H···O hydrogen bonds, π···π interactions and interactions involving the substituents can have a significant influence on the supramolecular arrays generated in the aggregation.

In a further study of benzaldehyde oximes, we have determined the crystal structures of four compounds, namely 3-chlorobenzaldehyde oxime, **1**, 4-fluorobenzaldehyde oxime, **2**, 2-nitrobenzaldehyde oxime, **3**, and 4-nitrobenzaldehyde oxime, **4**, from data collected at $T = 100$ K, see Scheme 1. The crystal structure of **4** has previously been determined from data collected at room temperature, and the same $P2_1/c$ phase was found in each case [23–25]. These earlier studies made no mention of the intermolecular interactions, aside from the classical hydrogen bonds involving the oxime atoms. Aims of this study were to further investigate the occurrence of $R_2^2(6)$ dimers and C(3) chains in non-salicylaldoxime derivatives, the importance of π(C=N)···π(phenyl) interactions in benzaldehyde oxime derivatives in general, and the influence of other weaker intermolecular interactions derived specifically from halo and nitro substituents.

2 Results and Discussion

2.1 General

The asymmetric unit of each compound, **1–4**, contains a single molecule. All four compounds crystallize in the monoclinic system: compounds **1**, **2** and **4** in space group $P2_1/c$ and compound **3** in $P2_1/n$, all with $Z = 4$. The geometry around the oxime moieties is (*E*) in all four molecules. Figure 2 illustrates the atom arrangements and numbering schemes. The interplanar angles between the substituents and their attached phenyl group are all less than 10° in compounds **1**, **2** and **4**, but in the *ortho*-substituted compound, **3**, all such angles are greater than 26°, due to steric hindrance between the nitro and oxime groups (Table 1). Details of the hydrogen bonding and other intermolecular interactions are provided in Table 2. The major intermolecular interactions in **1–4** involve the O13–H13···N12 hydrogen bonds. In **1** these generate C(3) chains which run parallel to the *b* axis formed by

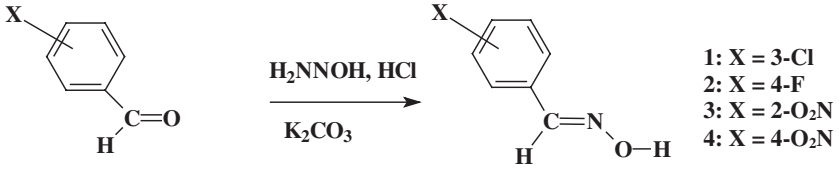

Scheme 1: Synthesis of **1–4.**

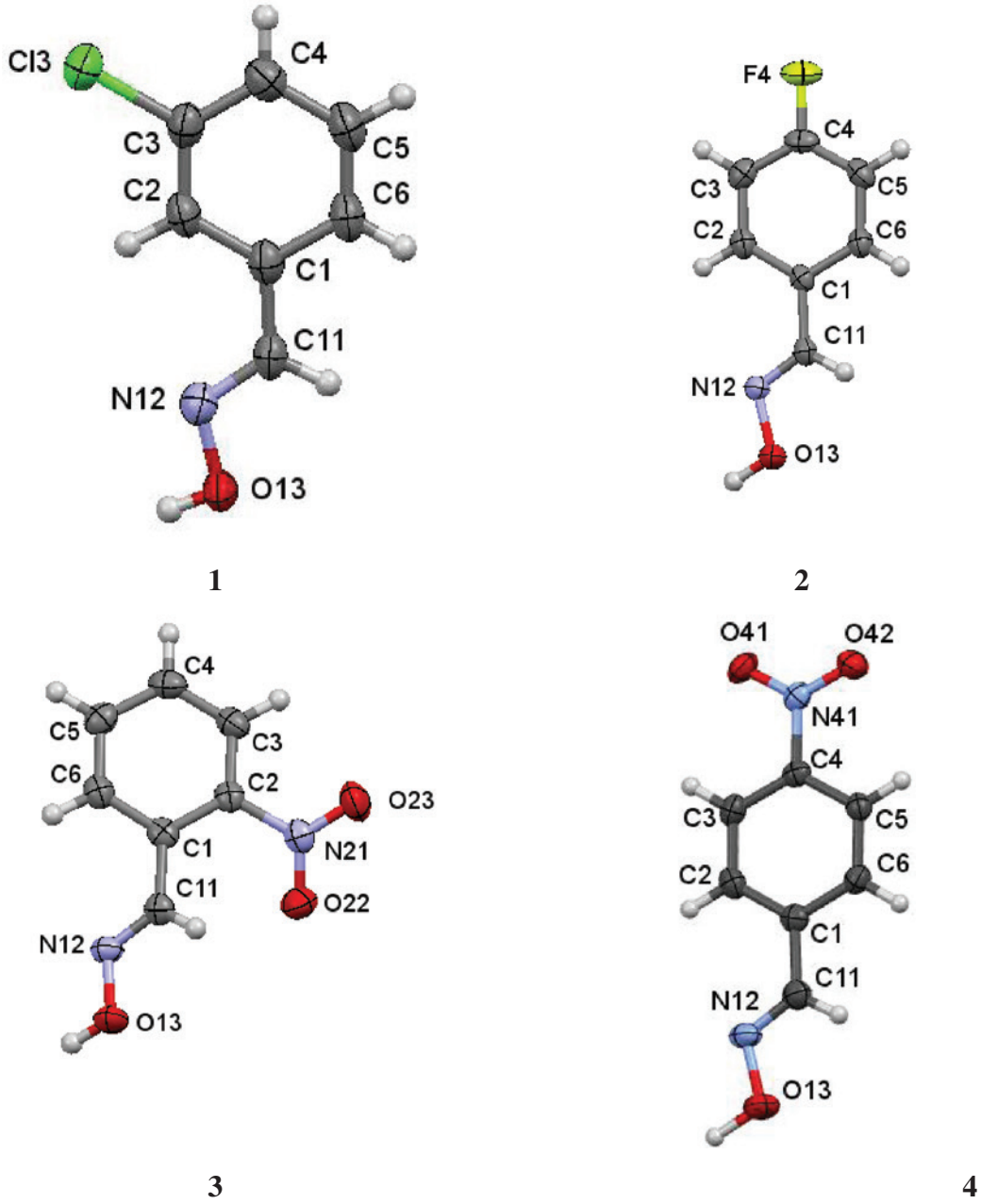

Fig. 2: Views of the asymmetric units of **1–4** with the atom numbering schemes. Displacement ellipsoids are drawn at the 80% probability level, hydrogen atoms as spheres with arbitrary radii.

Table 1: Interplanar angles (deg) for compounds **1–4**.

	Between oxime group and attached phenyl ring	Between nitro group and attached phenyl ring	Between oxime and nitro groups
1	7.60(1)		
2	9.63(1)		
3	37.82(1)	26.2(1)	39.26(1)
4	8.25(1)	3.86(1)	4.86(1)

the action of the screw axis at (1/2, *y*, 1/4) (Fig. 3), whilst in **2–4**, the O13–H13···N12 hydrogen bonds form $R_2^2(6)$ dimers across the centres of symmetry at (1/2, 0, 1/2), (1, 1/2, 1/2) and (1, $\bar{1}$, 1), respectively. Within the $R_2^2(6)$ dimers of compounds **2–4** there are O13–H13···O13 hydrogen bonds, with longer than usual H13···O13 distances, of 2.585(19), 2.636(18) and 2.59(2) Å, respectively, and small O13–H13···O13 angles, near 120°, see (Table 2). The involvement of pairs of the O13–H13···O13 hydrogen

Table 2: Geometric parameters and symmetry operations for hydrogen bonds and intermolecular interactions (Å, deg).[a]

Intermolecular hydrogen bonds

	D–H···A	D–H	H···A	D···A	D–H···A	Symmetry code
1	O13–H13···N12	0.85(3)	1.96(3)	2.8007(18)	177(3)	$-x+1, y+1/2, -z+1/2$
2	O13–H13···O13	1.00(2)	2.585(19)	3.2002(10)	119.7(13)	$-x+1, -y, -z+1$
2	O13–H13···N12	1.00(2)	1.88(2)	2.7991(11)	151.8(16)	$-x+1, -y, -z+1$
2	C3–H3···F4	0.95	2.58	3.4670(13)	156	$-x, y-1/2, -z+1/2$
2	C5–H5···F4	0.95	2.65	3.4416(13)	142	$-x, -y, -z$
2	C11–H11···O13	0.95	2.50	3.4229(13)	165	$-x+1, y+1/2, -z+1/2$
3	O13–H13···O13	0.921(19)	2.636(18)	3.2451(17)	124.3(13)	$-x+2, -y+1, -z+1$
3	O13–H13···N12	0.921(19)	1.937(19)	2.8016(13)	155.5(15)	$-x+2, -y+1, -z+1$
3	C3–H3···O13	0.95	2.47	3.3132(15)	148	$-x+3/2, y-1/2, -z+1/2$
3	C6–H6···O23	0.95	2.60	3.1744(15)	119	$-x-3/2, y-1/2, -z-3/2$
4	O13—H13···O13	0.89 (1)	2.68 (2)	3.2559(19)	124 (2)	$-x+1, -y-1, -z+1$
4	O13—H13···N12	0.89 (1)	1.99 (1)	2.8191(15)	154(2)	$-x+1, -y-1, -z+1$
4	C6—H6···O41	0.95	2.53	3.3032(16)	139	$x+1, y-1, z$
4	C11—H11···O41	0.95	2.42	3.1577(15)	134	$x+1, y-1, z$

Y–X···π interactions

	Y–X···Cg	X···Cg	X_{perp}	γ	Y–X···Cg	Y···Cg	Symmetry code
4	N41–O41···Cg1	3.8471(10)	3.480	25.25	65.05(6)	3.5105(11)(15)	$x, 1+y, z$
4	N42–O41···Cg1	3.3858(10)	3.345	8.89	85.57(7)	3.5105(11)	$x, 1+y, z$

π···π interactions[a]

	CgI···Cg(J)	Cg···Cg	α	β	γ	CgI_{perp}	CgJ_{perp}	Slippage	Symmetry code
2	Cg···Cg	3.7672(7)	0	24.8	24.8	3.4186(5)	3.4186(5)	1.583	$x, -1+y, z$
2	Cg···Cg	3.7672(7)	0	24.8	24.8	3.4186(5)	3.4185(5)	1.583	$x, 1+y, z$
3	Cg···Cg	3.6405(7)	0	15.6	15.6	3.5064(4)	3.5063(4)	0.979	$-1+x, y, z$
3	Cg···Cg	3.6405(7)	0	15.6	15.6	3.5063(4)	3.5064(4)	0.979	$1+x, y, z$

[a]α = Dihedral angle between planes I and J (deg); β = angle Cg(I)→Cg(J); γ = angle Cg(I)→Cg(J) vector and normal to plane J (deg); Cg···Cg = distance between ring centroids (Å); CgI_{Perp} = perpendicular distance of Cg(I) on ring J (Å); CgJ_{perp} = perpendicular distance of Cg(J) on ring I (Å).

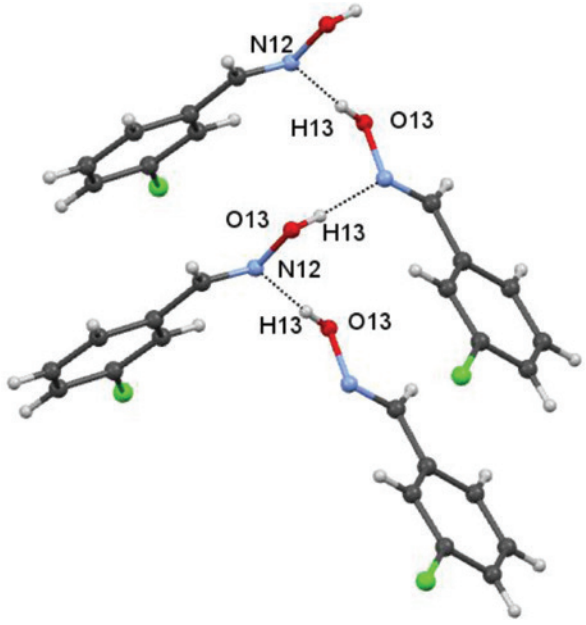

Fig. 3: The C3 chain in compound **1**, formed from C13–H13···N12 hydrogen bonds. Table 3 lists the symmetry operations.

bonds subdivides the $R_2^2(6)$ dimers into three rings – two $R_1^2(3)$ rings and one $R_2^2(4)$ ring. Such $R_1^2(3)$ and centrosymmetric $R_2^2(4)$ rings have been variously reported for organic molecules. Indeed a recent CCDC data base search revealed more than 500 entries of non-solvated structures having centrosymmetric H_2O_2 rings with H–O–H angles of 120° or less and H–O distances up to the sum of the contact radii, 2.72 Å, of oxygen and hydrogen. In particular, the literature search indicated that various aldoximes, but not all, possess similar sub-divided $R_2^2(6)$ rings, with much smaller H–O distances, e.g., less than 2.60 Å: examples include 4-$Me_2NC_6H_4CH$=NOH from room temperature data [CCDC codes MABZOX and 1208893: ref 26] and more from data at low temperatures [e.g. 2,3-Me_2-4-$MeOC_6H_2CH$=NOH: CCDC codes OKUHAD and 161452; ref 27]: 4-BrC_6H_4CH=NOH: CCDC codes BAGWOW and 181389: ref 28]. The data for compounds **2–4** are thus not unusual and do suggest that the O13–H13···O13 hydrogen bonds can be considered as contributing to the overall stability of the $R_2^2(6)$ dimers. Two views of each of the $R_2^2(6)$ dimers are

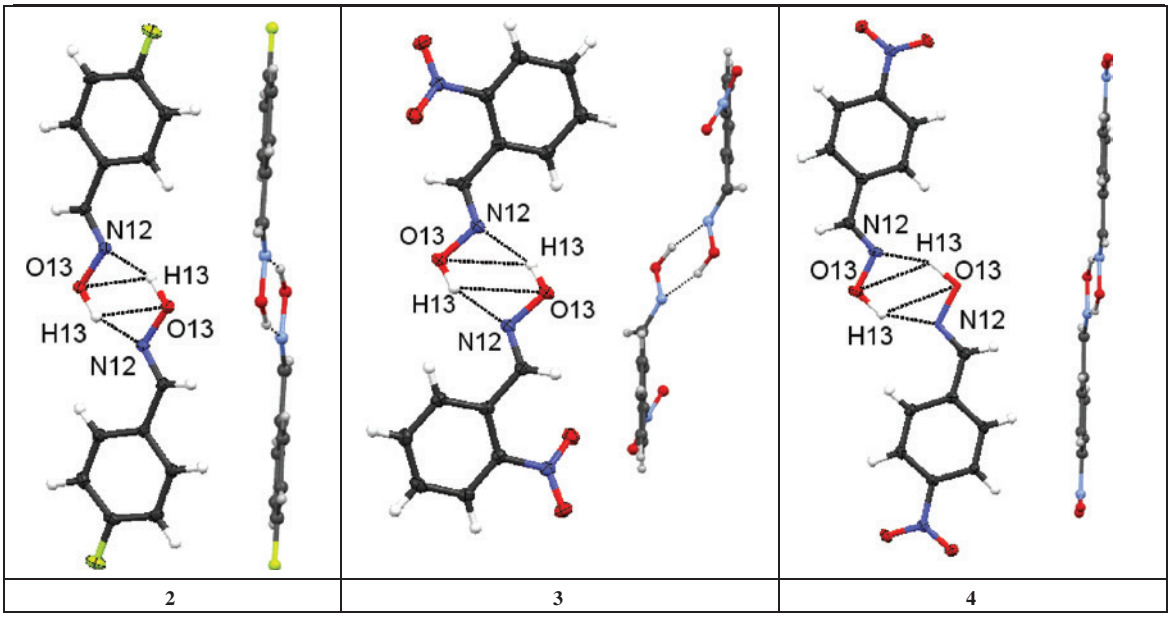

Fig. 4: Two views of the $R_2^2(6)$ dimers for compounds **2**, **3** and **4**.

shown in Fig. 4, one looking face-on and the other side-on to the parallel phenyl rings. The perpendicular distances between the parallel phenyl rings in the $R_2^2(6)$ dimers are 0.955, 2.609 and 0.751 Å, respectively in **2–4** (Fig. 4): the greater distance in compound **3** reflects the greater deviation of its oxime unit from the plane of its attached phenyl group as a consequence of steric hindrance between its groups in *ortho*-position.

Table 3 lists the percentage atom-atom contacts for all compounds.

2.2 Other intermolecular interactions in individual compounds

2.2.1 The chain-forming compound 1

Interactions in **1**, in addition to the C(3) chain forming O13–H13···N12 hydrogen bond, are (i) short Cl···Cl^{i} intermolecular contacts, which link the C3 chains: the Cl···Cl distance is 3.418(6) Å, just within the sum of the contact radii of 3.50 Å (symmetry code: i = $-x$, $-y$, $-z$), and (ii) π(C=N)···π(phenyl) interactions, with a Cg(C=N)···Cg(phenyl)^{ii} distance of 3.290(1) Å (Cg being the center of gravity of the phenyl ring): symmetry code: ii = x, $-1+y$, z) (Fig. 5). The π(C=N)···π(phenyl) interaction is more fully discussed in the Section: π(C=N)···π(phenyl) contacts below.

The Hirshfeld surface and Fingerprint (FP) plots [29, 30] for compound **1** are shown in Fig. 6. The C···C, Cl···Cl and N···H close contacts are designated as are the site of the π···π contacts. In the FP plot, the two spikes pointing southwest relate to N···H contacts including those making the C(3) chains; the high density of pixels near $d_i \approx d_e \approx 1.8$ Å is due to C···C contacts, and that close to the $d_i \approx d_e \approx 1.8$–2.0 Å region is due to Cl···Cl contacts, and the wings ending approximately at $(d_i; d_e) \approx (1.2; 1.8)$ Å are due to H···Cl contacts.

Table 3: Percentages of atom-atom contacts.

Compound	H···H	H···O/O···H	H···C/C···H	H···N/N···H	C···C	O···C/C···O	N···O/O···N	N···C/C···N	O···O
1	26.3	10.5	16.1	8.0	5.2	2.3	–	2.6	
2	32.0	11.3	13.4	10.3	9.1	1.0	0.7		
3	27.5	38.2	4.7	7.5	10.8	2.0	2.8	2.9	3.4
4	29.7	29.1	7.5	7.5	4.0	9.1	2.4	5.2	5.1

Compound	H···Cl/Cl···H	Cl···C/C···Cl	F···C/C···F	F···F	H···F/F···H
1	24.3	2.3			
2			2.1	2.1	17.6

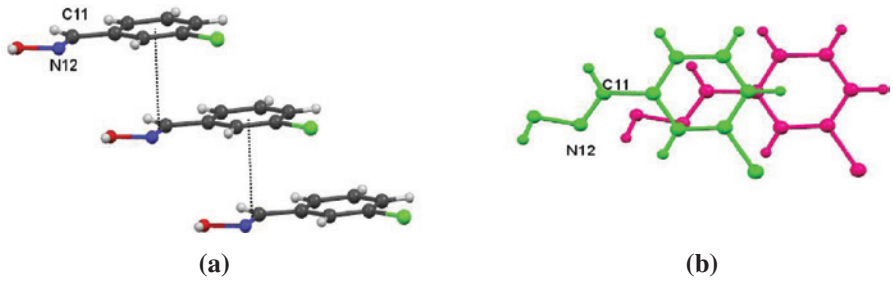

Fig. 5: Compound **1**. (a) Part of a stack of molecules formed from π(C=N) ··· π(phenyl) interactions. The Cg(C=N) ··· Cg^{i} (phenyl) distance is 3.290(1) Å (symmetry code: i = *x*, –1+*y*, *z*; (b) the overlap of the C=N and phenyl π systems in successive rows of the π(C=N) ··· π(phenyl).

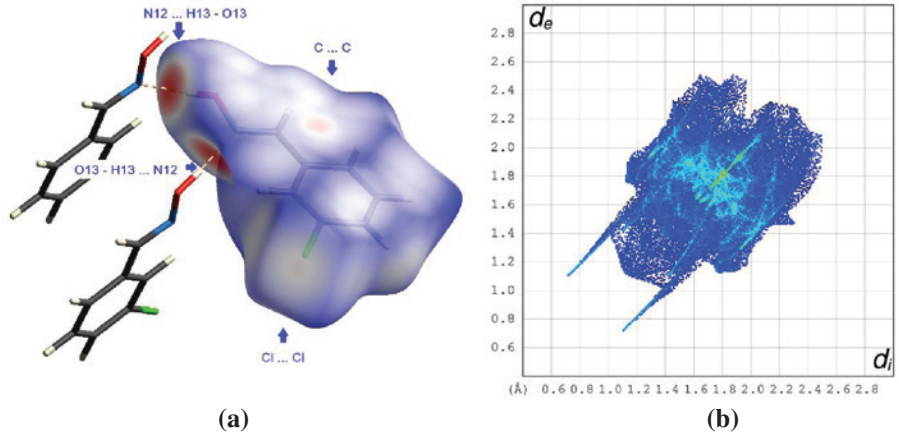

Fig. 6: Compound **1**. (a) View of the Hirshfeld surface mapped over d_{norm}: the set of two intense red area spots relate to N ··· H close contacts in forming the C3 chain; also designated are the sites of the C ··· C and π ··· π contacts; (b) the FP plot, the two spikes pointing southwest relate to N ··· H contacts including those making the C(3) chains; the high density of pixels near $d_i \cong d_e \cong 1.8$ Å are due to C ··· C and those close to $d_i \cong d_e \cong 1.8$–2.0 Å interval are due to Cl ··· Cl contacts, wings ending approximately at (d_i; d_e) ≅ (1.2; 1.8) Å are due to H ··· Cl contacts.

Compound **1** has the highest percentage of H ··· C/C ··· H contacts and the lowest percentage of H ··· H and H ··· O/O ··· H contacts of all four compounds studied here, see Table 3. There is also a high percentage of H ··· Cl/Cl ··· H contacts in compound **1**.

2.3 The compounds forming $R_2^2(6)$ dimers

2.3.1 Compound 2

In **2**, in addition to the O13–H13 ··· N12 and O13–H13 ··· O13 hydrogen bonds, there are weaker C11–H11 ··· O13, C3–H3 ··· F4 and C5–H5 ··· F4 hydrogen bonds, and π ··· π interactions. The overall structure can be conveniently considered to be formed from two substructures. Firstly, the $R_2^2(6)$ dimers are linked by the C5–H5 ··· F4 hydrogen bonds into chains, which are further linked by the π ··· π interactions into sheets, as illustrated in Fig. 7a. Within the sheets are $R_2^2(8)$ rings, arising from the C–H ··· F hydrogen bonds, as well as the $R_2^2(6)$ rings. The overlap of the π systems in successive layers of the π ··· π stacks is illustrated in Fig. 7b: the Cg ··· Cg^{i} distance is 3.7672 (7) Å, and the perpendicular distance between the planes is 3.4186(5) Å with a slippage of 1.583 Å (symmetry code: i = *x*, –1+*y*, *z*). The second sub-structure in compound **2** is a further sheet formed from combinations of C11–H11 ··· O13 and C3–H3 ··· F4 hydrogen bonds. Each of these hydrogen bonds individually generates C4 spiral chains, which run parallel to the *b* axis, formed by the action of the screw axis at (1/2, *y*, 1/4). Within this sheet is a network of $R_4^4(22)$ rings (Fig. 7c). Combination of the two different sheets generates a three-dimensional array.

Compound **2** has the highest percentage of H ··· H contacts, 32.0%, significantly higher than the sum, 21.8%, of fluorine contacts (H ··· F/F ··· H, F ··· C/C ··· F and F ··· F). The H ··· O/O ··· H, H ··· C/C ··· H, and H ··· N/N ··· H contacts all are ca 10%.

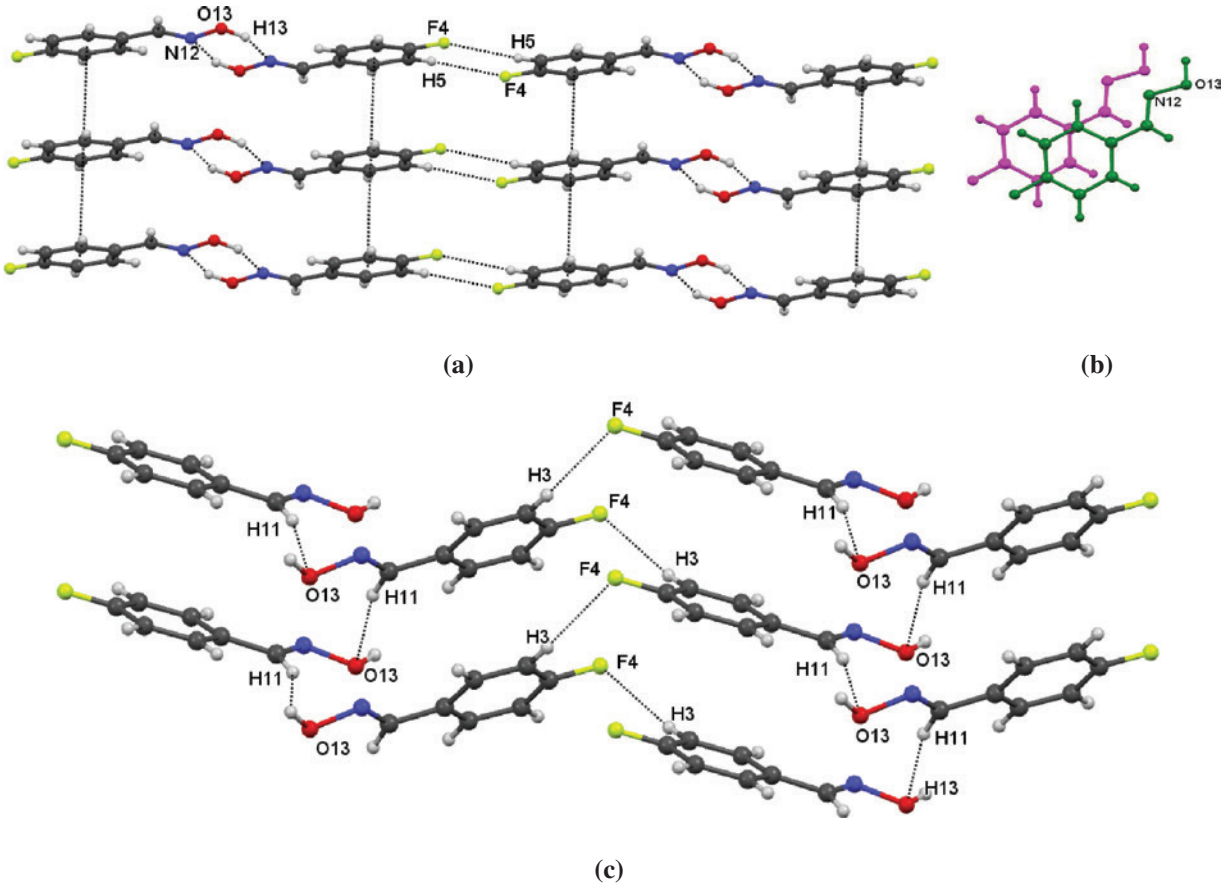

Fig. 7: Compound **2**. (a) Part of a sheet formed from linking the $R_2^2(6)$ dimers with C5–H5 · · · F4 hydrogen bonds and π · · · π interactions; (b) the overlap of the π systems in successive layers of the π · · · π stack, shown in Fig. 7a; (c) part of a sheet formed from linkages using C11–H11 · · · O13 and C3–H3 · · · F4 hydrogen bonds. Details of the intermolecular interactions are displayed in Table 3.

The three other 4-halobenzaldehyde oximes, (*E*)-4-XC_6H_4CH=N–OH (X=Cl [31], Br [28] and I [20]) were also shown to form $R_2^2(6)$ dimers.

2.3.2 Compound 3

The intermolecular interactions in compound **3**, in addition to the dimer forming O13–H13 · · · N12 and C3–H3 · · · O13 hydrogen bonds, are C6–H6 · · · O23(nitro) hydrogen bonds and π · · · π interactions. The $R^2_2(6)$ dimers are linked by the C3–H3 · · · O13 and C6–H6 · · · O23 hydrogen bonds into sheets. These sheets are composed of a network of $R_3^3(12)$ and $R_4^4(26)$ rings, complemented by $R_2^2(6)$ rings (Fig. 8a). The sub-structure generated from linking the $R_2^2(6)$ dimers with the π · · · π interactions is illustrated in Fig. 8b. The overlap of the π systems in successive layers of the stack is shown in Fig. 8c: the Cg · · · Cg^i distance is 3.6405(7) Å, the perpendicular distance between the planes is 3.5064 (5)Å and the slippage is 0.979 Å (symmetry code: –1 + *x*, *y*, *z*). The distance between N21(nitro group) and $O22^i$ (nitro group) in successive layers of the stack is 3.0658(13) Å, which is at the sum of the contact radii and thus does not suggest any significant nitro group – nitro group interaction. There is however a short O13(hydroxyl) · · · $O23^{ii}$(nitro) separation of 2.928(13) Å, well within the sum of the contact radii of 3.04 Å (symmetry code: ii = 3/2–*x*, 1/2 + *y*, 1/2–*z*).

2.3.3 Compound 4

There are major differences between the contacts found in compounds **3** and **4**, which are both nitro phenyl derivatives. In compound, **4**, in addition to the O13–H13 · · · N12 and C3–H3 · · · O13 hydrogen bonds, which form the $R_2^2(6)$ dimers, there are other intermolecular interactions solely involving the nitro group atoms. Three distinct types of nitro group interactions are found

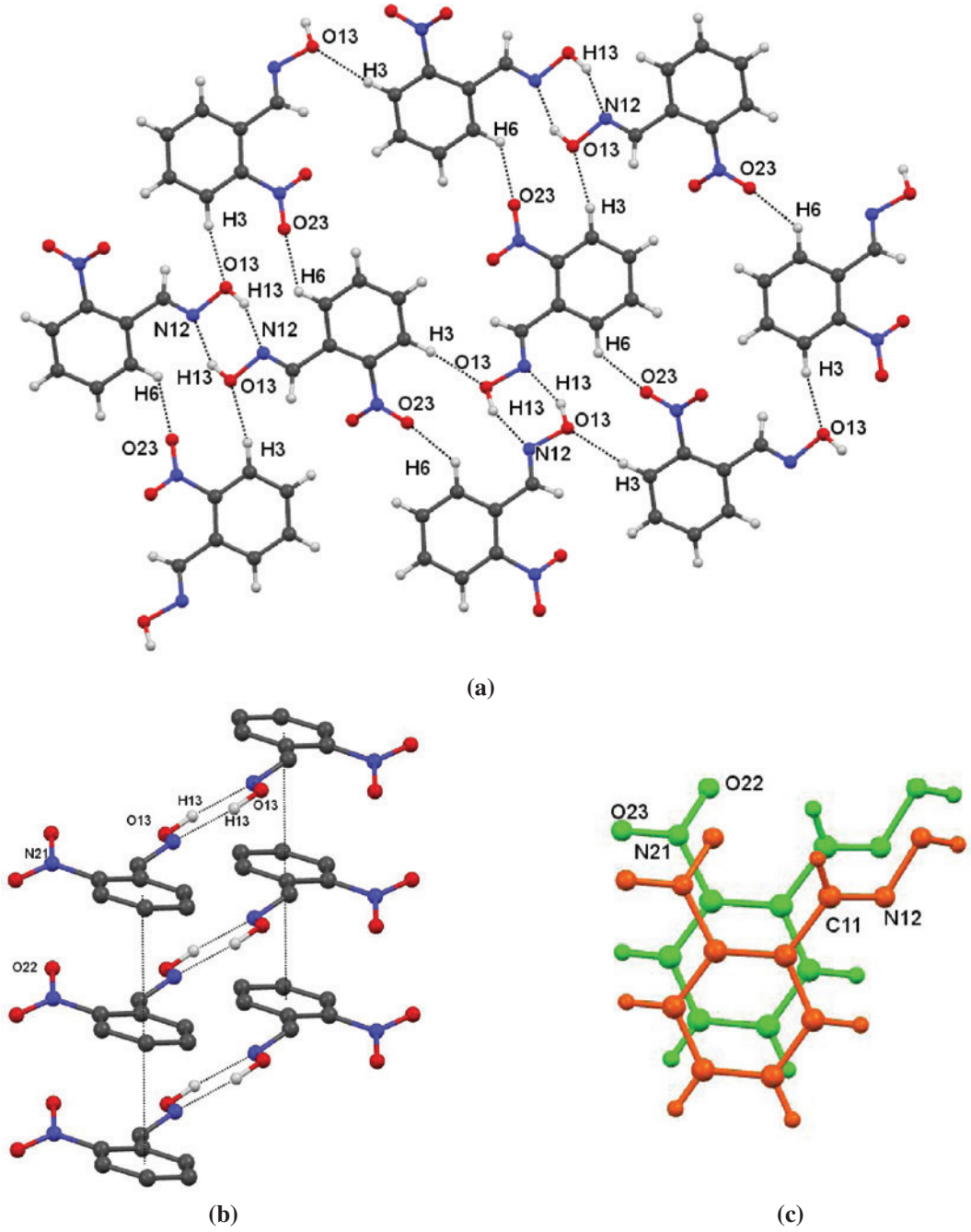

Fig. 8: Compound **3**. (a) Part of a sheet of molecules formed from combination of O13–H13···N12, C3–H3···O13 and C6–H6···O23 hydrogen bonds; (b) part of a double π···π stack, formed from the $R_2^2(6)$ dimers; (c) the overlap of the π systems in the stacks shown in Fig. 8b. Details of the intermolecular interactions are displayed in Table 3.

in compound **4**, all of which link the $R_2^2(6)$ dimers into more elaborate sub-structures: (i) the nitro group oxygen atom, O41, acts as the acceptor in C6–H6···O41^{i} and C11–H11···O41^{ii} hydrogen bonds (Table 2). (ii) nitro···nitro group interactions [32], with a O42···N41^{iii} separation of 2.8641(13) Å (symmetry code: iii = $-x$, 1/2 + y, 1/2–z), and (iii) both the oxygen atoms of the nitro group are used in N41–O41···π^{iii} and N41–O42···π^{iii}, with O41···π^{iii} and O42···π^{iii} distances of 3.8471(10) and 3.3858(10) Å, respectively (symmetry code iii = x, 1 + y, z). The first of these interactions, involving the C6–H6···O41 and C11–H11···O41 hydrogen bonds, link the $R_2^2(6)$ dimers into tilted two-molecule wide columns as illustrated in Fig. 9a. Within the columns are $R_2^2(6)$ and $R_4^4(26)$, as well as $R_2^2(6)$ rings. The nitro groups at the ends of the $R_2^2(6)$ dimers are involved in the nitro···nitro group

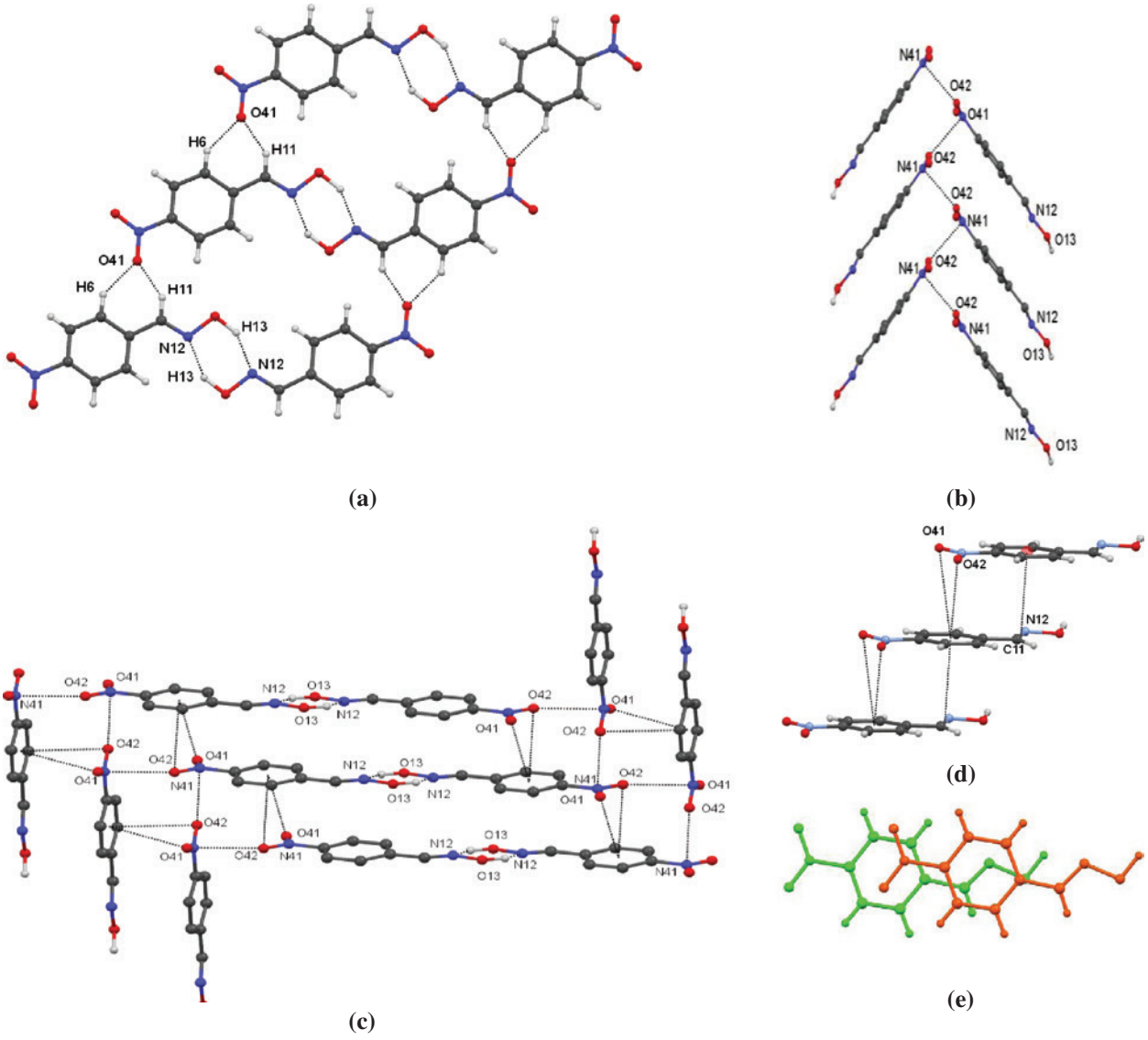

Fig. 9: Compound **4**. (a) Part of a two-molecular wide tilted sheet formed from linking the $R_2^2(6)$ dimers by C6–H6 · · · O41 and C11–H11 · · · O41 hydrogen bonds; (b) the Chevron style arrangement arising from the nitro-nitro group interactions; (c) a part of the arrangement generated from linking the $R_2^2(6)$ dimers by N41–O41 · · · π, N21–O42 · · · π and the nitro-nitro interaction; (d) part of the stack obtained from combination of the N41–O41 · · · π, N21–O42 · · · π and π (C=N) · · · π(phenyl) interactions; (e) the overlap of molecules in the stack shown in Fig. 9d. Details of the intermolecular interactions are displayed in Table 3.

contacts with O41 · · · O42^{v} and O42 · · · N41^{vi} distances of 2.9294(11) and 2.8641(13) Å, respectively, both within the appropriate sums of the contact radii of 3.04 and 3.07 Å, respectively (symmetry codes: v = $-x$, $-1/2+y$, $1/2-z$; vi = $-x$, $1/2+y$, $1/2-z$). These nitro · · · nitro group interactions, which provide a Chevron-type arrangement, are illustrated in Fig. 9b. Figure 9c shows the arrangement obtained from linking the $R_2^2(6)$ dimers by N41–O41 · · · π, N41–O42 · · · π and the nitro · · · nitro interactions. Within this arrangement are layers of $R_2^2(6)$ dimers in which the C=N unit of the oxime in one layer sits above a phenyl ring in a successive layer, with a Cg(C=N) · · · Cg(phenyl) distance of 3.406 Å, which suggests a π(C=N) · · · π(phenyl) interaction (Fig. 9d and e). This is longer than the equivalent distance found in compound **1** and, in addition, this positioning of the C=N unit may be serendipitous and a consequence of the other interactions in the column, for example the N41–O41 · · · π, N41–O42 · · · π interactions (Fig. 9d). However, while it is not so clear cut as the situation in compound **1**, such a π(C=N) · · · π(phenyl) interaction is stabilizing as discussed below in the chapter on π(C=N) · · · π(phenyl) interactions.

2.4 Comparison of the structures of the three isomeric nitrobenzaldehyde oximes

Comparisons of the structures of the three isomeric mononitrobenzaldehyde oximes can be made, as the structure of 3-nitrobenzaldehyde oxime, **5**, has been briefly reported from data collected at room temperature [33]. The *ortho*- and *meta*-isomers, compounds **3** and **5**, have similar sets of intermolecular interactions, which are significantly different from those of the *para*-isomer, **4**. While only the classical hydrogen bonds forming the $R_2^2(6)$ dimers were mentioned in the published report on **4** [33], a deeper analysis of the structure has indicated a strong $\pi\cdots\pi$ interaction, with a Cg$\cdots$Cg distance of 3.7738(14) Å, a distance between parallel phenyl rings of 3.4677(10) Å and a slippage of 1.489 Å, similar to the situation in the *ortho*-isomer, **3**. Also as in compound **3**, the nitro group atoms are only involved in C–H$\cdots$O hydrogen bonds, but rather than the sheet found in compound, **3**, only a two-molecule wide column is generated from the $R_2^2(6)$ dimers and the available C–H$\cdots$O hydrogen bonds in **5**.

No π(C=N)$\cdots\pi$(phenyl) interaction is apparent in **5**, as the relevant Cg$\cdots$Cg distance is >4.4 Å.

2.5 Hirshfeld surfaces and FP plots for compounds, 2–4

Views of the Hirshfeld surface [29, 30] for compounds, **2–4**, which form $R_2^2(6)$ dimers, are illustrated in Fig. 10. For each compound, red areas are designated corresponding to O–H$\cdots$N and N$\cdots$H–O and other contacts, including the O$\cdots$O and N$\cdots$O close contacts found in compound **4**. The FP plots for these three compounds are illustrated in Fig. 11. The similarity of the three FP plots is apparent: any differences between the plots arise from the different percentages of H$\cdots$X (X=H, O, N, Cl or F) contacts for each molecule. The N$\cdots$H close contacts are responsible for the pair of sharp spikes ending at d_e/d_i ca 1.2 Å (d_e and d_i are the axes of the FP plots). Close to these spikes are other, less-sharp, peaks, which correspond to O$\cdots$H contacts, and the area within the spikes appearing as the comb-like teeth is due to H$\cdots$H close contacts

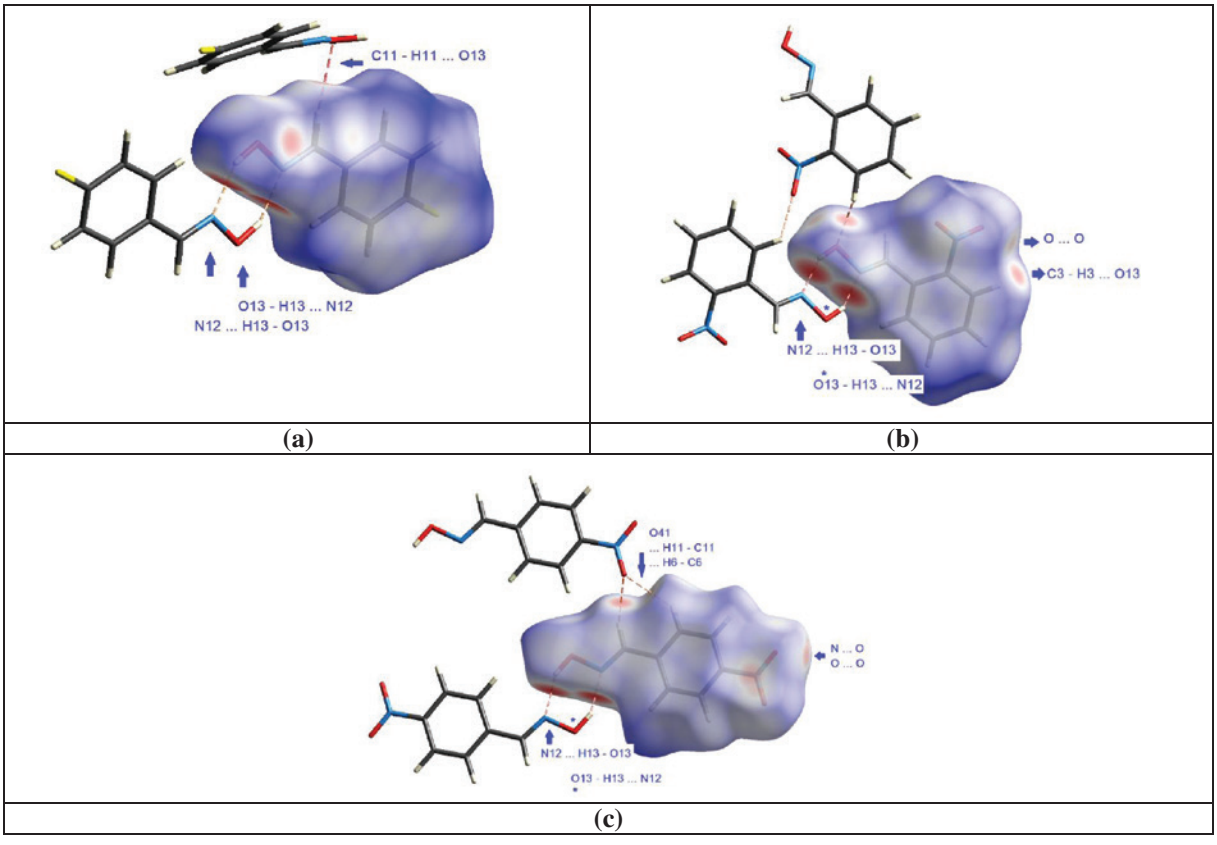

Fig. 10: Views of the Hirshfeld surface mapped over d_{norm} for compounds (a) **2**, (b) **3** and (c) **4**, forming $R_2^2(6)$ rings. In each compound, red areas relating to O–H$\cdots$N and N$\cdots$H–O and other contacts are designated.

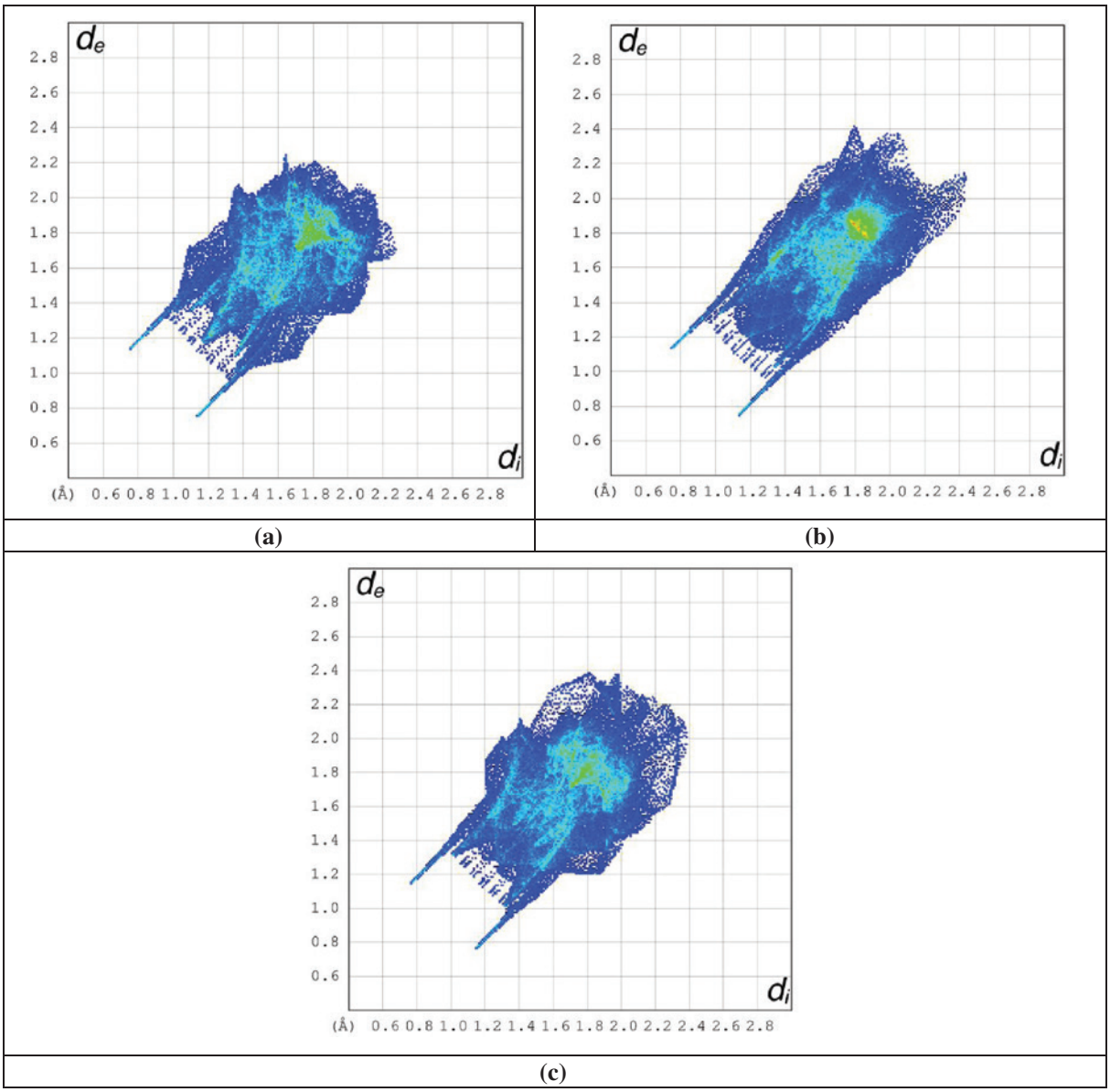

Fig. 11: FP plots for compounds (a) **2**, (b) **3** and (c) **4**, which form the $R_2^2(6)$ dimers. The N···H close contacts result in the pair of sharp spikes in the FP plot, ending at d_e/d_i ca.1.2 Å. Very close to those spikes are other, less-sharp, peaks which arise from O···H contacts. The area within the spikes appearing as "teeth of a comb" is due to H···H close contacts involving the H atoms of the hydroxyl group of the oxime. The higher percentage of C···C contacts in compound **3** are indicated by the higher pixel frequency at d_e / $d_i \cong 1.8$ Å as shown by the light green and red areas.

involving the hydroxyl group of the oxime. The small teeth-like peaks shown in Fig. 11 for the $R_2^2(6)$ dimer-forming compounds and their absence in the FP plot for the C3 chain-forming compound **2**, shown in Fig. 6, clearly point to major differences in the structures. A breakdown of the H···X (X=H, O, N, and F) contacts in compound **2**, is illustrated in Fig. 12. The percentage atom···atom contacts in **2–4** are shown in Table 3. As expected for the two nitro derivatives, **3** and **4**, the combined percentages of close contacts involving oxygen are high.

2.6 π(C=N)···π(phenyl) interactions

The clear indication of a π(C=N)···π(phenyl) interaction in compound **1**, and the less clear indication in compound **4**, led to an investigation of similar interactions in other oximes with Cg(C=N)···Cg(phenyl) distances up to 3.30 Å. Among the compounds found were the high pressure $P2_1/n$ phase of salicylaldoxime [SALOXM-08] [34], the high pressure $I2/a$ phase of 3-*t*-butylsalicylaldoxime [NIRJII-07] [35] and benzene-1,3,5-tris(*N*-hydroxy-methanimine)

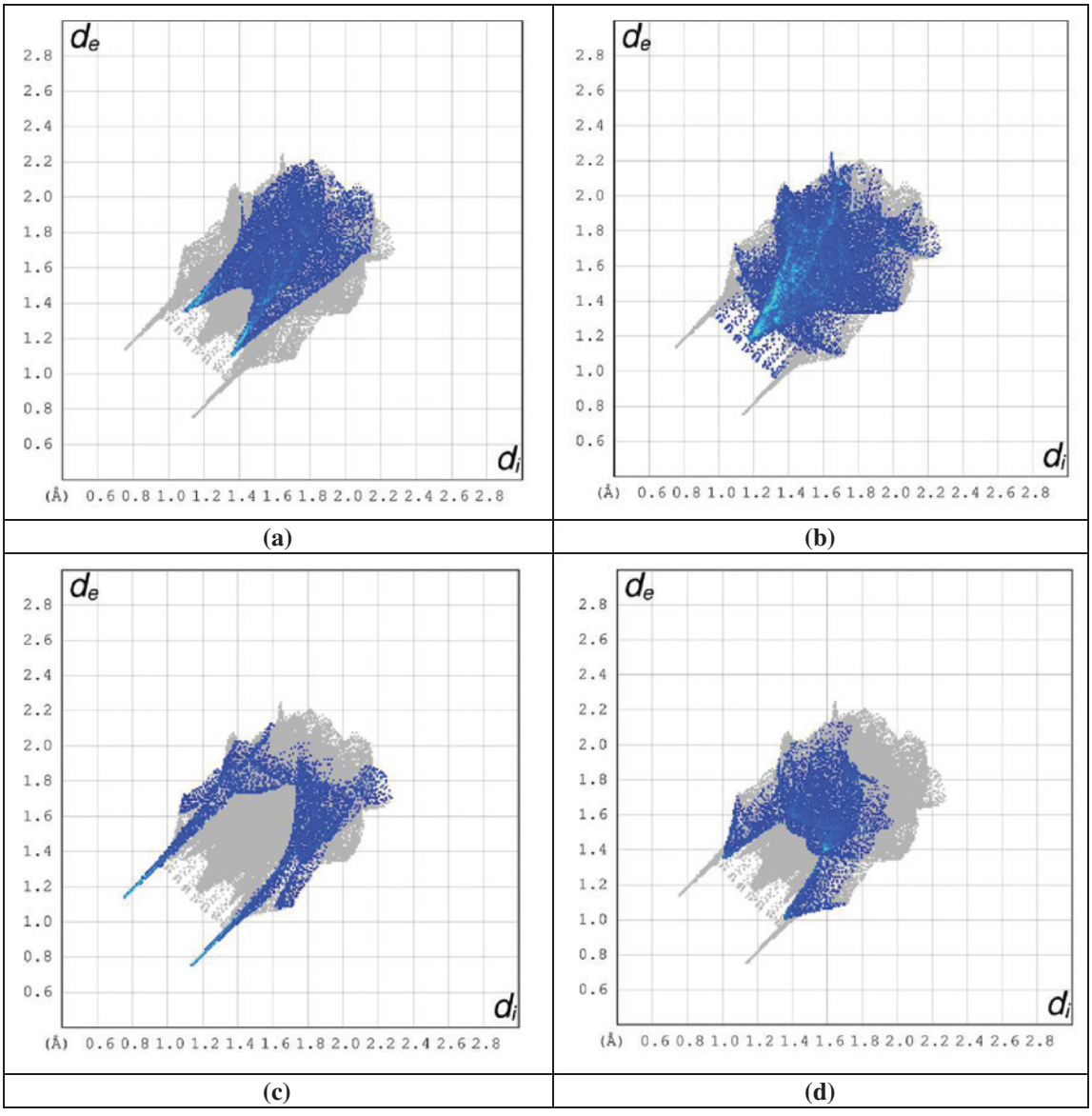

Fig. 12: Partial FP plots for **2** showing pixels due to (a) F···H, (b) H···H, (c) N···H and (d) O···H contacts.

[ADOJEK] [36]. Oxime ethers, such as, 1-(salicylidene-oxy)-2-(3-methoxysalicylidenesmino-oxy)ethane [FOJROM] [37] were also found with short Cg(C=N)···Cg((phenyl) distances. A search on 12-06-2018 of the CCDC data base of compounds possessing C=N–X fragments (X=OH, OR, NR^1R^2 etc) with Cg(C=N)···Cg(phenyl) distances less than 3.30 Å, revealed more than 80 hits. Extending the Cg(C=N)···Cg(phenyl) distance beyond 3.30 to 4.0 Å brought in many more compounds. Short Cg(C=N)···Cg(phenyl) distances were found to be very much less common for compounds with -CH=N–OR (R=H or organyl) fragments, compared to compounds with C=N–NXY fragments.

2.6.1 Theoretical calculations on the potential of π(C=N)···π(phenyl) interactions in compound 1

A theoretical study of the potential π(C=N)···π(phenyl) interactions was carried out on compound **1**, using initially a stacked dimer, extracted from the CIF (structure A in Fig. 13). Figure 13 shows the various structures and sub-structures, and their associated calculated interaction energies. To separate the two possible intermolecular interactions in the dimer A – the π(CN)···π(phenyl) interaction and the OH···N hydrogen bond – two additional dimers were constructed: replacement of the CH=N(OH) moiety by a hydrogen atom in the upper molecule removes

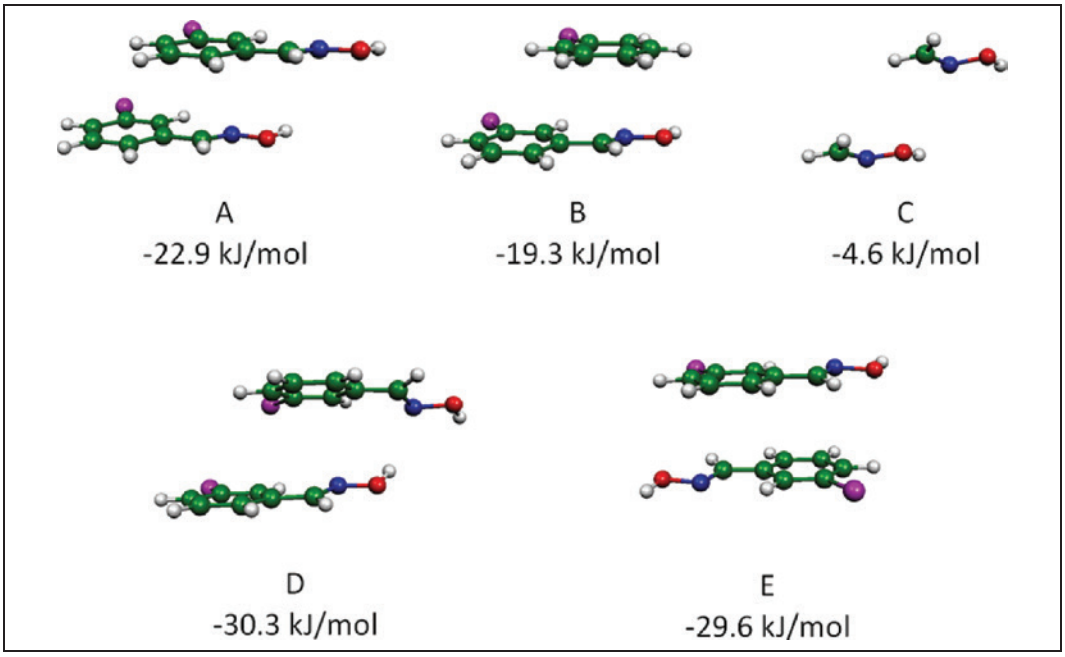

Fig. 13: Stuctures, used in the theoretical calculations on the π(CN) ⋯ π(phenyl) interaction in compound **1**, and their energies.

the OH ⋯ N interaction (structure B) and replacement of the chlorophenyl unit by a hydrogen atom in both molecules removes the potential π(CN) ⋯ π(phenyl) interaction (structure C). The interaction energy of structure A (–22.9 kJ mol^{-1}) shows that there is a considerable and attractive interaction between the two molecules at the experimental geometry. However, only part of this attraction can be attributed to the π(CN) ⋯ π(phenyl) interaction, as there is also an OH ⋯ N interaction in the dimer. When optimizing the geometry (structure D), this interaction makes the structure less parallel. Structure E, where one of the molecules is rotated to avoid this OH ⋯ N interaction, remains parallel and has an interaction energy of –29.6 kJ mol^{-1}. Assuming that this interaction energy results from two CN ⋯ π interactions, one such interaction is estimated to be –14.8 kJ mol^{-1}.

Structures B and C aim to eliminate the π(CN) ⋯ π(phenyl) and OH ⋯ N interactions. The sum of the interaction energies of B and C (–23.9 kJ mol^{-1}) is not far off from that of the full dimer (–22.9 kJ mol^{-1}), so it seems reasonable to assume that the interaction energy of the full dimer is a sum of the π(CN) ⋯ π(phenyl) and OH ⋯ N interactions. These results suggest that the π(CN) ⋯ π(phenyl) interaction accounts for –19.3 kJ mol^{-1}. This is a bit higher than the –14.8 kJ mol^{-1} estimated above, but is probably an overestimation, as there are more attractive interactions in this dimer than just the π(CN) ⋯ π(phenyl) interaction (for example, with the hydrogen atom of the upper molecule above the ring of the lower molecule in structures A and B). In summary, the calculations support that the CN ⋯ π interaction is attractive, with a considerable magnitude estimated to be in the range of –15 to –18 kJ mol^{-1}.

Table 4 shows a breakdown of the interaction energy into separate contributions using sSAPT0. The sSAPT0 interaction energies are in reasonable agreement with the PBE0 values. The results show that dispersion is relatively more important in A and B compared to C, and electrostatics are more important in C.

3 Experimental

3.1 Synthesis and crystallization

The compounds, **1–4**, were prepared by refluxing the corresponding aldehyde with hydroxyamine in an aqueous solution containing potassium carbonate, rather than pyridine, following a published procedure [45]. They were purified by recrystallization from methanol solutions.

3-Chlorobenzaldehyde oxime, **1:** m.p. 64–65°C [46]. 4-Fluorobenzaldehyde oxime, **2:**. m.p. 85–87°C (lit [http://synquestlabs.com/product/id/53507.html]: m.p. 85–86°C). 2-Nitrobenzaldehyde oxime, **3:** m.p. 97–98°C (lit. [https://www.alfa.com/en/catalog/A14565/]: m.p. 98–102°C). 4-Nitrobenzaldehyde oxime, **4:** m.p. 123–124°C (lit. [https://www.alfa.com/en/catalog/L09144/]: m.p. 122–125°C).

Table 4: Crystal data.

	1	2	3	4
Crystal data				
Chemical formula	C_7H_6ClNO	C_7H_6FNO	$C_7H_6N_2O_3$	$C_7H_6N_2O_3$
M_r	155.58	139.13	166.14	166.14
Crystal system, space group	Monoclinic, $P2_1/c$	Monoclinic, $P2_1/c$	Monoclinic, $P2_1/n$	Monoclinic, $P2_1/c$
Temperature, K	100	100	100	100
a, b, c, Å	12.1214(7), 4.4332(2), 13.6946(8)	14.2137(5), 3.7672(1), 11.9364(4)	3.6405(1), 13.4466(6), 14.8993(7)	6.2083(2), 4.8431(2), 24.3013(8)
β, deg	109.283(6)	99.210(3)	95.086(4)	94.986(3)
V, Å^3	694.62(7)	630.90(4)	726.48(5)	727.91(5)
Z	4	4	4	4
Radiation type	Mo$K\alpha$	Mo$K\alpha$	Mo$K\alpha$	Mo$K\alpha$
μ, mm^{-1}	0.5	0.1	0.1	0.1
Crystal size, mm^3	0.20×0.05×0.03	0.20×0.10×0.02	0.15×0.05×0.03	0.06×0.05×0.01
Data collection				
Diffractometer	(a)	(a)	(a)	(b)
Absorption correction	(c)	(c)	(c)	(c)
No. of measured/independent/ observed [$I > 2\sigma(I)$] reflections	14977/1591/1381	13530/1443/1349	16152/1669/1549	8656/1670/1462
R_{int}	0.068	0.029	0.064	0.021
$(\sin\theta/\lambda)_{max}$, Å^{-1}	0.649	0.649	0.649	0.649
Refinement				
No. of reflections	1591	1443	1669	1670
No. of parameters	95	95	113	113
No. of restraints	0	0	0	1
H atom treatment	(d)	(d)	(d)	(d)
$R[F^2 > 2\sigma(F^2)]$, $wR(F^2)$, S	0.041, 0.118, 1.08	0.033, 0.101, 1.09	0.033, 0.089, 1.07	0.036, 0.102, 1.08
$\Delta\rho_{max/min}$, e Å^{-3}	0.53, −0.37	0.35, −0.21	0.31, −0.16	0.38, −0.23
CCDC No	1846653	1846654	1846655	1856711

(a) Rigaku FRE+equipped with VHF Varimax confocal mirrors and an AFC12 goniometer and HyPix 6000 detector diffractometer; (b) XtaLAB AFC12 (RCD3): Kappa single diffractometer; (c) Multi-scan CrysAlis Pro 1.171.39.30d (Rigaku Oxford Diffraction, 2017) Empirical absorption correction using spherical harmonics, implemented in SCALE3 ABSPACK scaling algorithm; (d) H atoms treated by a mixture of independent and constrained refinement. Computer programs used: CrysAlis PRO 1.171.39.30d [38], Oscail [39], Shelxt [40], ShelXle [41], Shelxl2017/1 [42], Mercury [43], Platon [44].

3.2 Crystallography

Crystal data, data collection and structure refinement details are summarized in Table 5 [38–44]. In each case the oxime group has an (*E*) geometry. In all compounds the oxime hydroxyl hydrogen atoms were refined and their positions checked on a final difference map where all atom positions lie within the maximum contour level. All other hydrogen atoms were refined as riding atoms at a distance of 0.95Å.

The Hirshfeld surfaces and two-dimensional fingerprint (FP) plots [29, 30] were generated using Crystal Explorer 3.1 [29, 30]. The Hirshfeld surface mapped over d_{norm} is scaled in the range −0.68 to 1.17.

Table 5: Breakdown of the interaction energies of the different dimers using sSAPT0

Structure	Electrostatics	Exchange	Induction	Dispersion	Total
A	−21.0	50.6	−4.5	−50.7	−25.7
B	−19.7	50.0	−4.5	−47.3	−21.5
C	−2.6	4.6	−0.7	−3.8	−2.6
D	−24.36	45.02	−6.26	−45.37	−30.98
E	−19.07	43.41	−4.05	−53.27	−32.98

3.3 Theoretical study of the π(C=N)···π(phenyl) interaction in compound 1

Hydrogen geometries were optimised with the BLYP-D3 density functional (BLYP [47, 48] augmented with Grimme's D3 dispersion correction [49] in conjunction with the def2-SVP basis set [50] using Orca [51], keeping

all other atoms at the experimental geometry. Interaction energies were computed with PBE0-D3 (the hybrid PBE0 functional [52] augmented with D3) and the ma-def2-TZVP basis set [50, 53]. The counterpoise procedure [54] was used to eliminate BSSE. As the heavy atoms are at the crystallographic positions, deformation energies were omitted. The interaction energies were thus computed as follows:

$$\Delta E = E_A^{\{AB\}}(AB) - E_A^{\{AB\}}(AB) - E_A^{\{AB\}}(AB) \quad (1)$$

Here, the superscript {*AB*} denotes that all calculations employ the dimer basis set, and the attributes in round brackets, (*AB*), denote that all calculations employ the dimer geometry.

Additional calculations at the PBE0-D3/ma-def2-TZVP level employing the counterpoise procedure. The structures were additionally analyzed with Symmetry-Adapted Perturbation Theory (SAPT) [55], which calculates the interaction energy directly without computing the dimer and monomer energies. We employed a scaled version, sSAPT0 [56], of the simplest truncation of the SAPT expansion (SAPT0), with a truncated aug-cc-pVDZ basis set labelled jun-cc-pVDZ (previously called aug-cc-pVDZ' [57]), using Psi4 [58]. This level of theory was recommended as a good-performing, efficient level of SAPT [56].

4 Conclusions

The crystal structures and the results of the Hirshfeld surface analysis of four aldoximes, $XC_6H_4CH{=}N{-}OH$ (X = 3-Cl (**1**), 4-F (**2**), 2-O_2N (**3**) and 4-O_2N (**4**), are reported. The strong classical O13–H13 ··· N12 hydrogen bonds involving the oxime moiety generate C3 chains in compound **1**, in contrast to the $R_2^2(6)$ dimers in compounds **2–4**. Pairs of O13–H13 ··· O13 hydrogen bonds subdivide the $R_2^2(6)$ dimers into two $R_1^2(3)$ and one $R_2^2(4)$ rings. Weaker interactions involving the substituents in **1–4** influence the supramolecular arrays. Important in compound **1**, and to a lesser extent in **4**, are π(C=N) ··· π(phenyl) interactions. A data base search has indicated that short Cg(C=N) ··· Cg(phenyl) distances, <3.3 Å, are present in various compounds, including other oximes. A theoretical study was carried out at the BLYP-D3/def2-DZVP and PBE0/ma-def2-TZVP levels. Overall, the calculations indicate that the π(C=N) ··· π(phenyl) interaction in **1** is attractive, with a considerable magnitude of 14–18 kJ mol^{-1}.

5 Supporting information

CCDC 1846653–1846655 and 1856711 for compounds **1–4**, respectively, contain the supplementary crystallographic data for this paper. These data can be obtained free of charge from The Cambridge Crystallographic Data Centre *via* www.ccdc.cam.ac.uk/data_request/cif.

The crystallographic CIFs are also given as supplementary material available online (DOI: 10.1515/znb-2018-0222).

Acknowledgements: The authors thank the National Crystallographic Service, University of Southampton, UK, for the data collection, and for their help and advice. LRG thanks the Portuguese Foundation for Science and Technology (FCT) UID/Multi/04546/2013.for support.

References

[1] E. Abele, R. Abele, E. Lukevics, *Chem. Heterocycl. Compds*. **2018**, *44*, 769.
[2] A. Nikitjuka, A. Jirgensons, *Chem. Heterocycl. Compds*. **2014**, *49*, 1544.
[3] R. Martinez-Pascual, S. Meza-Reyes, J. L. Vega-Baez, P. Merino-Montiel, J. M. Padron, A. Mendoza, S. Montiel-Smith, *Steroids* **2017**, *122*, 24.
[4] H. L. Qin, J. Leng, B. G. M. Youssif, M. W. Amjad, M. A. G. Raja, M. A. Hussain, Z. Hussain, S. N. Kazmi, S. N. A. Bukhari, *Chem. Bio. Drug Des*. **2017**, *90*, 443.
[5] C. Canario, S. Silvestre, A. Falcao, G. Alves, *Curr. Med. Chem*. **2018**, *25*, 660.
[6] G. Huang, H. R. Zhao, Q. Q. Meng, Q. J. Zhang, J. Y. Dong, B. Q. Zhu, S. S. Li, *Eur. J. Med. Chem*. **2018**, *143*, 166.
[7] H. Dai, J. Chen, G. Li, S. S. Ge, Y. J. Shi, Y. Fang, Y. Ling, *Bioorg. Med. Chem. Lett*. **2017**, *27*, 950.
[8] S. Y. Zhao, K. Li, Y. Jin, J. Lin, *Eur. J. Med. Chem*. **2018**, *144*, 41.
[9] P. Yadav, K. Lal, P. Rani, S. Mor, A. Kumar, *Med. Chem. Res*. **2017**, *26*, 1469.
[10] J. Kozlowska, B. Potaniec, B. Zarowska, M. Aniol, *Molecules* **2017**, *22*, 1485.
[11] A. M. Mohassab, H. A. Hassan, D. Abdelhamid, M. Abdel-Aziz, K. N. Dalby, T. S. Kaoud, *Bioorg. Chem*. **2017**, *75*, 242.
[12] D. E. Lorke, H. Kalasz, G. A. Petroianu, K. Tekes, *Curr. Med. Chem*. **2008**, *15*, 743.
[13] V. A. Voicu, H. Thiermann, F. S. Radulescu, C. Mircioiu, D. S. Miron, *Basic. Clin. Pharmacol. Toxicol*. **2010**, *106*, 73.
[14] M. Katalinic, A. Zandona, A. Ramic, T. Zorbaz, I. Primozic, Z. Kovarik, *Molecules* **2017**, *22*, 1234.
[15] Z. Radic, T. Dale, Z. Kovarik, S. Berend, E. Garcia, L. Zhang, G. Amitais, C. Green, B. Radi, B. M. Duggan, D. Ajami, P. Taylor, *Biochem. J*. **2013**, *450*, 231.
[16] M. Sorensen, E. H. J. Neilson, B. L. Moller, *Mol. Plant*, **2018**, *11*, 95.
[17] V. Bertolasi, G. Gilli, A. C. Veronese, *Acta Crystallogr*. **1982**, *B38*, 502.

[18] E. A. Bruton, L. Brammer, F. C. Pigge, C. B. Aakeröy, D. S. Leinen, *New J. Chem*. **2003**, *27*, 1084.
[19] J. N. Low, L. M. N. B. F. Santos, C. F. R. A. C. Lima, P. Brandão, L. R. Gomes, *Eur. J. Chem*. **2010**, 61.
[20] C. B. Aakeroy, A. S. Sinha, K. N. Epa, P. D. Chopada, M. M. Smit, J. Desper, *Cryst. Growth Des*. **2013**, *13*, 2687.
[21] J. N. Low, J. L. Wardell, C. F. da Costa, M. V. N. de Souza, L. R. Gomes, *Eur. J. Chem*. **2018**, *9*, 151.
[22] M. C. Etter, *Acc. Chem. Res*. **1990**, *23*, 120.
[23] M. Tonogaki, T. Kawata, S. Ohba, Y. Iwata, I. Shibuya, *Acta Crystallogr*. **1993**, *B49*, 1031.
[24] V. Sharutin, *CSD Communication* code: 1045607, **2016**.
[25] L. Brehm, K. J. Watson, *Acta Crystallogr*. **1972**, *B28*, 3646.
[26] F. Bachechi, L. Zambonelli, *Acta Crystallogr*. **1972**, *B28*, 2489.
[27] E. Pindelska, T. M. Krygowski, R. Anulewicz-Ostrowska, M. K.Cyranski, J. Nowacki, *J. Phys. Org. Chem*. **2001**, *14*, 764.
[28] A. D. Ward, V. R. Ward, E. R. T. Tiekink, *Z. Kristallogr. NCS* **2001**, *216*, 583.
[29] S. K. Wolff, D. I. Grimwood, J. J. McKinnon, M. J. Turner, D. Jayatilaka, M. A. Spackman, Crystal Explorer (version 3.1), The University of Western Australia, Perth (Australia) **2012**.
[30] J. J. McKinnon, M. A. Spackman, A. S. Mitchell, *Acta Crystallogr*. **2004**, *B60*, 627.
[31] J. T. Mague, Y. El Bakri, CSD private Communication, CBALOS02: 1506791, **2016**.
[32] M. Daszkiewicz, *CrystEngComm* **2013**, *15*, 10427.
[33] A. Abbas, S. R. Hussain, N. Hafeez, A. Badshah, A. Hasan, K. M. Lo, *Acta Crystallogr*. **2010**, *E66*, o1130.
[34] P. A. Wood, R. S. Forgan, D. Henderson, S. Parsons, E. Pidcock, P. A. Tasker, J. E. Warren, *Acta Crystallogr*. **2006**, *B62*, 1099.
[35] P. A. Wood, R. S. Forgan, A. R. Lennie, S. Parsons, E. Pidcock, P. A. Tasker, J. E. Warren, *CrystEngComm*, **2008**, *10*, 239.
[36] C. B. Aakeroy, A. S. Sinha, K. N. Epa, C. L. Spartz, J. Desper, *Chem. Commun*. **2012**, *48*, 11289.
[37] S. Akine, T. Taniguchi, W. Dong, S. Masubuchi, T. Nabeshima, *J. Org. Chem*. **2005**, *70*, 1704.
[38] Rigaku Oxford Diffraction, Rigaku Corporation, Tokyo, Japan, **2017**.
[39] P. McArdle, K. Gilligan, D. Cunningham, R. Dark, M. Mahon, *CrystEngComm* **2004**, *6*, 303.
[40] G. M. Sheldrick, *Acta Crystallogr.* **2015**, *A71*, 3.
[41] C. B. Hübschle, G. M. Sheldrick, B. Dittrich, *J. Appl. Crystallogr.* **2011**, *44*, 1281.
[42] G. M. Sheldrick, Shelxl-2017/1, University of Göttingen, Göttingen (Germany) **2017**.
[43] Mercury, Crystal Structure Visualisation, Exploration and Analysis made Easy, CCDC, **2018**.
[44] A. L. Spek, *Acta Crystallogr.* **2009**, *D65*, 148.
[45] *Vogel´s Textbook of Practical Organic Chemitry*, 5th edition, revised by B. S. Furniss, A. J. Hannaford, P. W. G. Smith, A. R. Tatchell, Longman Group UK Limited, London, **1989**, p. 1259.
[46] L. Zhang, J. C. Chung, T. D. Costello, I. Valvis, P. Ma, S. Kauffman, R. Ward, *J. Org. Chem*. **1997**, *62*, 2466.
[47] A. D. Becke, *Phys. Rev*. **1988**, *A38*, 3098.
[48] C. Lee, W. Yang, R. G. Parr, *Phys. Rev*. **1988**, *B37*, 785.
[49] S. Grimme, J. Antony, S. Ehrlich, H. Krieg, *J. Chem. Phys*. **2010**, *132*, 154104.
[50] F. Weigend, R. Ahlrichs, *Phys. Chem. Chem. Phys*. **2005**, *7*, 3297.
[51] F. Neese, *Wiley Interdiscip. Rev.: Comput. Mol. Sci.* **2012**, *2*, 73.
[52] C. Adamo, V. Barone, *J. Chem. Phys*. **1999**, *110*, 6158.
[53] J. Zheng, X. Xu, D. G. Truhlar, *Theor. Chem. Acc*. **2011**, *128*, 295.
[54] S. F. Boys, F. Bernardi, *Mol. Phys*. **1970**, *19*, 553.
[55] B. Jeziorski, R. Moszynski, K. Szalewicz, *Chem. Rev*. **1994**, *94*, 1887.
[56] T. M. Parker, L. A. Burns, R. M. Parrish, A. G. Ryno, C. D. Sherrill, *J. Chem. Phys*. **2014**, *140*, 094106.
[57] E. G. Hohenstein, R. M. Parrish, C. D. Sherrill, J. M. Turney, H. F. Schaefer, *J. Chem. Phys*. **2011**, *35*, 174107.
[58] J. M. Turney, A. C. Simmonett, R. M. Parrish, E. G. Hohenstein, F. Evangelista, J. T. Fermann, B. J. Mintz, L. A. Burns, J. J. Wilke, M. L. Abrams, N. J. Russ, M. L. Leininger, C. L. Janssen, E. T. Seidl, W. D. Allen, H. F. Schaefer, R. A. King, E. F. Valeev, C. D. Sherrill, T. D. Crawford, *Wiley Interdiscip. Rev.: Comput. Mol. Sci*. **2012**, *2*, 556.

Supplementary Material: The online version of this article offers supplementary material (https://doi.org/10.1515/znb-2018-0222).